Optimization of aerodynamic and acoustic performances of supersonic civil transports

Bijan Mohammadi
University of Montpellier, Montpellier, France

Keywords *Optimization techniques, Flow, Aerodynamics, Acoustic properties*

Received March 2003
Revised September 2003
Accepted December 2003

Abstract *This paper presents a shape optimization problem under acoustic, aerodynamic and geometric constraints. The acoustic specification concerns the generated sonic boom. The aim is to see the validity of incomplete sensitivities when a nonlinear CFD model is coupled with a nonlinear wave transport model to define pressure rise on the ground.*

1. Introduction

In shape design for transonic aircraft under cruise conditions, multi-criteria aspects mainly concern the aerodynamic and elastic characteristics of the aircraft. For instance, the aim can be to reduce the drag at given lift and with given maximum by-section thickness, which would ensure structural realizability. Shape optimization for civil supersonic transport includes another main ingredient: the control of the generated sonic boom (Whitham, 1952). This makes the problem harder than in the transonic case as drag and sonic boom reductions are by nature incompatible (in supersonic regime low drag geometries are sharp and have high boom level as shocks are attached then).

A large effort is currently being made on the improvement of the potential of supersonic transport. As an example, in the United States, the DARPA Quiet Supersonic Platform (QSP) program is directed towards development and validation of critical technology for long-range advanced supersonic aircraft with substantially reduced sonic boom, reduced takeoff and landing noise, and increased efficiency relative to current generation supersonic aircraft. Improved capabilities include supersonic flight over land without adverse sonic boom consequences with boom overpressure rising less than 0.3 pounds per square feet (psf) (about 14 Pa), increased unrefueled range approaching 6,000 nmi, gross take-off weight approaching 100,000 lb (about 50 tons), increased area coverage and lower overall operational cost.

Similar efforts are taken in Europe. In France, the Committee for Scientific Orientation for Supersonic Transport directs studies on the feasibility of the next generation of Concorde jetliner.

This work has been supported by the French Committee for Scientific Orientation for Supersonic Transport and the Center for Turbulence Research at Stanford University. The geometry of the SSBJ has been provided by Dassault Aviation Company. The author would like to thank in particular B. Stoufflet, M. Mallet, Ph. Rostand and G. Rogé of Dassault Aviation for their suggestions. He would also like to thank Prof. S. Candel, A. Dervieux, D. Jeandel, P. Moin and O. Pironneau for their interests in this work realization. Thanks also to Dr J. Alonso, M. Fatica and B. Koobus for the scientific interactions. Many thanks to Dr. M. Wang for his helpful feedback on this manuscript. The author is grateful to M. Chethik, C. Gichane-Bell, M. Lomuljo-Bautista and D. Micheal for their assistance during his stay at CTR.

International Journal of Numerical Methods for Heat & Fluid Flow
Vol. 14 No. 7, 2004
pp. 893-909

0961-5539
DOI 10.1108/09615530410546272

2. Sonic boom

The sound heard on the ground as a "sonic boom" is the sudden onset and release of pressure after the buildup by the shock wave or "peak overpressure". The change in pressure caused by sonic boom is only a few psf – about the same pressure change we experience on an elevator as it descends two or three floors – in a much shorter time period. It is the magnitude of this peak overpressure that describes a sonic boom.

There are two types of booms: N-waves and U-waves. The N-wave is generated from steady flight conditions, and its pressure wave is shaped like the letter "N". N-waves have a front shock to a positive peak overpressure which is followed by a linear decrease in the pressure until the rear shock returns to ambient pressure. The U-wave, or focused boom, is generated from maneuvering flights, and its pressure wave is shaped like the letter "U". U-waves have positive shocks at the front and rear of the boom in which the peak overpressures are increased compared to the N-wave. Therefore, in principle, supersonic civil transport in cruise condition involves only N-waves. And this is what we observe in the present simulations.

In all case, for today's supersonic aircraft in normal operating conditions, the peak overpressure varies from less than 1 to about 10 psf for an N-wave boom (15-150 Pa). Peak overpressures for U-waves are amplified two to five times the N-wave, but this amplified overpressure impacts only a very small area when compared to the area exposed to the rest of the sonic boom. Therefore, shape optimization in cruise conditions leading to a reduction of the N-wave boom is fundamental.

The intensity and width of a sonic boom path depend on the physical characteristics of the aircraft and how it is operated. In general, the greater an aircraft's altitude, the lower the overpressure on the ground. Greater altitude also increases the boom's lateral spread, exposing a wider area to the boom. Overpressures in the sonic boom impact area, however, will not be uniform. Boom intensity is greatest directly under the flight path, progressively weakening with greater horizontal distance away from the aircraft flight track. This means that the characterization of the boom can mainly use the information along the symmetry line, along the flight path, on the ground.

Depending on the aircraft's altitude, sonic booms reach the ground 2-60 s after flyover. However, not all booms are heard at ground level. The speed of sound at any altitude is a function of air temperature. A decrease or increase in temperature results in a corresponding decrease or increase in sound speed. Under standard atmospheric conditions, air temperature decreases with increased altitude. This temperature gradient helps bend the sound waves upward. Therefore, for a boom to reach the ground, the aircraft speed relative to the ground must be greater than the speed of sound at the ground.

3. Governing equations

The flow in the regions close to the aircraft, or the near field, is computed using the Euler system for gas dynamics in conservation form. The solution method is based on a finite volume Galerkin method and is described by Mohammadi (1994). The variables at the lower boundary of this domain are then used to define waveform parameters which are propagated to the ground using the waveform parameter method (Thomas, 1972). A schematic of the approach is shown in Figure 1.

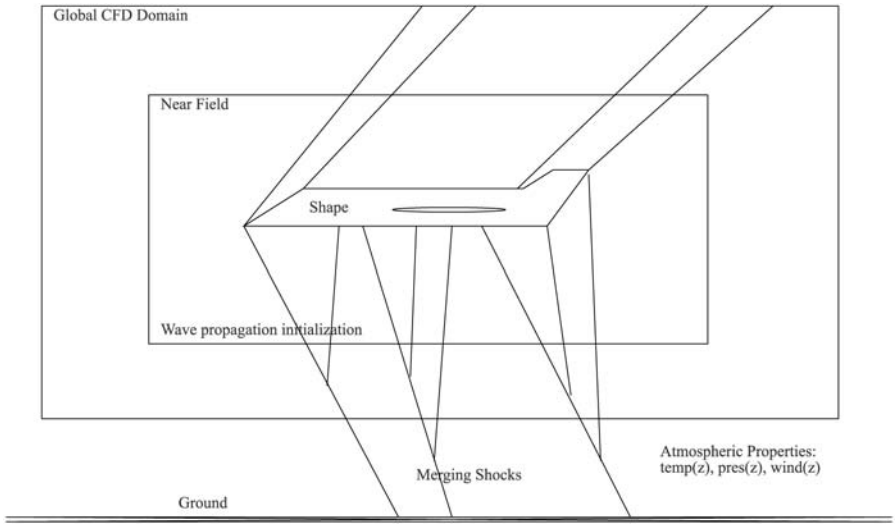

Figure 1.
Shock waves pattern and illustration of the near field CFD computation domain and the initialization of the wave propagation method with CFD predictions

3.1 Waveform parameter method

To propagate the near-field perturbations to the ground, we use the waveform propagation method (Thomas, 1972). The method is briefly described below. It is based on the solution of three ODE for the waveform parameters m_i (slope of the waveform segment), Δp_i (pressure rise across shock at the juncture of waveform segments i and $i-1$) and λ_i (time duration of waveform segment i):

$$\frac{\mathrm{d}m_i}{\mathrm{d}t} = C_1 m_i^2 + C_2 m_i,$$

$$\frac{\mathrm{d}\Delta p_i}{\mathrm{d}t} = \frac{1}{2} C_1 \Delta p_i (m_i + m_{i-1}) + C_2 \Delta p_i,$$

$$\frac{\mathrm{d}\lambda_i}{\mathrm{d}t} = -\frac{1}{2} C_1 (\Delta p_i + \Delta p_{i+1}) - C_1 m_i \lambda_i,$$

where

$$C_1 = \frac{\gamma + 1}{2\gamma} \frac{a_0}{p_0 c_\mathrm{n}},$$

$$C_2 = \frac{\mathrm{d}W}{\mathrm{d}t}, \quad W = \frac{1}{2} \log \left(\frac{a_0^3 \rho_0}{c_\mathrm{n}^2 A} \right),$$

where subscript 0 denotes ambient quantities, W is a nondimensional quantity that involves the speed at which a wave propagates normal to itself (c_n), the ambient sound speed (a_0), wind velocities and the ray tube area (A) (with dimension in $ML^{-2}T^{-1}$). These are given functions of altitude.

The solution of this ensemble is possible if initial distributions of the quantities are available. The initialization comes from the near field solution of the three dimensional CFD code. More precisely, the segments in our implementation correspond to an *a priori* uniform discretization along the flight path close to the symmetry plane of the aircraft. The values of the variables for this discretization come from the near field CFD values by interpolation. In our approach, the discretization along this path is finer than the one used for the CFD solution.

A segment is removed when the corresponding λ_i goes to 0. This means that the shock has coalesced with another one. In the same way, the slope m_i has to remain positive. This implies a projection step during the integration. We made extra hypothesis on the atmospheric distribution between flight altitude and ground, with in particular a zero wind velocity (i.e. $c_n = a_0$, a_0 being the ambient sound speed).

4. CAD-free shape parameterization

We use a CAD-free control space to specify shape deformations (Mohammadi and Pironneau, 2001). In this approach, all the nodes of the surface mesh over the shape are control parameters. One particularity of this parameterization comes from the fact that, unlike in a CAD-based parameter space, regularity requirements have to be specified and handled by the user. Indeed, if the shape is described using a CAD tool and if we use the same parameterization to specify the deformations, the two entities belong to the same space in terms of regularity.

From a practical point of view, this inconvenience is compensated by the fact that a CAD-based parameter space might not be suitable for optimization. In fact, our experience shows that optimization in the CAD-free framework helps improve the CAD definition of the shape. This is interesting as the final shape has to be expressed through CAD in all cases. Concerning mesh dependency of the optimization, the same remark holds when using a CAD-based parameter space. Indeed, it is obvious that the optimization might converge to different shapes in different CAD-based parameter spaces. Finally, new generation of CAD tools are able to fit CAD parameters into a surface mesh if the initial correspondence between CAD parameters and surface mesh is known. Theoretical justification for the introduction of smoothing operators for the CAD-free parameter space comes from the consistant approximation theory (Polak, 1997).

From a mathematical point of view, the importance of a smoothing step can also be understood by the following argument.

Suppose Γ is a surface in a domain $\Omega \in R^3$ and suppose we want shape variations $\delta x \in C^1(\Gamma)$. From Sobolev inclusions, we know for instance that in 2d $H^{5/2}(\Gamma) \subset C^1(\Gamma)$. In the context of shape optimization, applying to a C^1 shape Γ a gradient method does not necessarily produce a $C^1(\Gamma)$ variation δx. Actually, in applications with shocks the variation is rather in $L^2(\Gamma)$ (Mohammadi and Pironneau, 2001) and therefore we need to project the variations into $H^{5/2}(\Gamma)$ for instance.

The variations $(\delta\tilde{x})$ can be projected on $H^m(\Gamma)$ by solving a PDE of order $2m$ on Γ, such as (in 2d) $u^{(2m)} = -\delta\tilde{x}$.

Analysis suggests to use a fourth order operator (Mohammadi and Pironneau, 2001). From a numerical point of view, a second order elliptic system with a discontinuity capturing operator for the definition of the viscosity gives satisfactory results. Furthermore, it is a good idea to use an operator which leaves unchanged

regions where the deformation is already smooth enough. Second order operators are of course more localizing than fourth order operators.

4.1 Regularity and minimizing sequences

We give here a simple example to illustrate the loss of regularity in the construction of minimizing sequences in infinite dimension. The loss of regularity is related to the fact that the gradient of the functional has necessarily less regularity than the parameter.

Suppose that the functional $J(x)$ is a quadratic function of a parameter x $J(x) = (Ax - b)^2$ with $x \in H_0^1(\Omega)$, $b \in L^2(\Omega)$ and $A : H^1(\Omega) \rightarrow L^2(\Omega)$ where $\Omega \subset \{\mathbb{R}\}^n$. The gradient $\text{grad}_x J = 2A^{\text{T}}(Ax - b) \in H^{-1}(\Omega)$ has less regularity than x, therefore, an iterative scheme like the method of descent with step size ρ, $x^{m+1} - x^m = -\rho\, \text{grad}_x J = -2\rho A^{\text{T}}(Ax - b) \in V$ deteriorates the regularity of x. We, therefore, need to project (engineer would say smooth) the variation into $H^1(\Omega)$. This situation is similar to what happens with the CAD-free parameterization where a surface is represented by a large number (infinite) of independent points.

Now suppose the parameter belongs to a finite dimensional parameter space, as for instance with a polynomial definition of a surface. When we consider as parameter the coefficient of the polynomial, changes in the polynomial coefficients do not change the regularity as the new parameter will always belong to the same polynomial space. If the surface is parameterized by two (or several) polynomials, we, however, need to add regularity conditions for the junctions between the polynomials. We recover here the link introduced by the smoothing operator between parameter coefficients. This situation is similar to what happens with a CAD-based parameterization.

The smoothing can also be seen as a modification of the scalar product $(\cdot,\cdot)_0$ natural to Calculus of Variation, i.e. the scalar product of L^2 by a more elaborate one, such as $(\nabla\cdot,\nabla\cdot)_0$. It has a preconditioning effect in the sense that it dissipates localized high frequencies. From this standpoint at the discrete level, smoothing replaces a descent algorithm such as

$$j^{n+1} = j^n - \rho(\text{grad}_x j^n, \text{grad}_x j^n)_0$$

by

$$j^{n+1} = j^n - \rho(\text{grad}_x j^n, \text{grad}_x j^n)_M$$

where M is a preconditioning matrix.

In practice, we define the following "local" smoother over the shape:

$$(I - \varepsilon(\delta\tilde{x})\Delta)\delta\tilde{x} = \delta x, \tag{4.1}$$

$$\delta\tilde{x} = 0 \quad \text{on constrained frontiers},$$

where $\delta\tilde{x}$ is the smoothed shape variation for the shape nodes and δx is the variation given by the optimization tool. This system is solved iteratively and ε is set to 0 if

$$\frac{\delta_{ij}(\delta\tilde{x})}{(\delta\tilde{x})_{\text{T}}} < 10^{-3}, \tag{4.2}$$

where $\delta_{ij}(\delta\tilde{x})$ is the difference between the variations of the two nodes of each segment of a surface triangle and $(\delta\tilde{x})_{\text{T}}$ the mean variation on this triangle.

Once ($\delta\tilde{x}$) is known, we have to spread these variations over the mesh. Several algorithms are available for this task. We require the deformation method to preserve the positivity and orientation of the elements. In particular, we use a pseudo-elasticity algorithm combining compression and torsion springs (Farhat *et al.*, 1998).

5. Gradient evaluation

We consider two types of functionals: those using shape based information and those involving informations away from the shape. Examples of these are given by, for the first type, aerodynamic coefficients such as lift and drag coefficients or geometric quantities such as the volume and the maximum by-section thickness of the aircraft and for the former type the sonic boom defined by ground pressure signature.

There is a major difference between these two classes concerning the evaluation of sensitivities. Indeed, we will see that the first class is suitable for the use of the so-called incomplete sensitivity technique while a functional involving information on the ground requires the linearization of state equations.

5.1 Incomplete sensitivities

One of the main purposes of this paper is to see if we can use, for sonic boom reduction, a redefinition of the cost function compatible with incomplete sensitivity evaluations. Indeed, in the past we have applied this approximation to functionals involving aerodynamic coefficients. The redefinition is designed to be only used for sensitivity evaluation.

We recall briefly the incomplete sensitivity approach. Consider a general simulation loop linking the control parameter x to a functional J:

$$J(x) : x \rightarrow q(x) \rightarrow U(q(x)) \rightarrow J(x, q(x), U(q(x))), \tag{5.1}$$

where q represents all geometrical entities and U all state related variables. The gradient of J with respect to x is:

$$\frac{\mathrm{d}J}{\mathrm{d}x} = \frac{\partial J}{\partial x} + \frac{\partial J}{\partial q}\frac{\partial q}{\partial x} + \frac{\partial J}{\partial U}\frac{\partial U}{\partial x}. \tag{5.2}$$

The major part of the cost of this evaluation is due to $\partial U/\partial x$ in the last term.

Consider the following context for shape optimization:

- both the cost function and control space are defined on the shape (or on some part of it);
- J is of the form

$$J(x) = \int_{\text{shape}} f(x)g(U)\,\mathrm{d}\gamma,$$

- the local curvature of the shape is not too large (this needs to be quantified for each cases, for a wing typically we consider regions away from leading and trailing edges).

If these requirements hold, we can use an incomplete evaluation of this gradient, neglecting the sensitivity with respect to the state in (5.2). This does not mean that a precise evaluation of the state is not necessary, but that for a small change in the shape

the state will remain almost unchanged, while geometrical quantities have variations of the same order as the shape variation.

5.1.1 Illustrations of incomplete sensitivities. A first simple example concerns the application of the incomplete sensitivity technique to the evaluation of the sensitivity of functionals involving the solution of the following Burger equation:

$$u_t + 0.5(u^2)_x = \mu x u, \quad \text{on }]a, 1[, \quad u(a) = 1, \quad u(1) = -0.8. \tag{5.3}$$

We consider the steady solution of equation (5.3) and take the left hand side frontier a as control parameter. Suppose the functional is $J(a) = au_x(a)$, the gradient is given by

$$J_a(a) = u_x(a) + au_{xa}(a).$$

We are in the validity domain for incomplete sensitivities. Without computing the solution, it is clear from the equation that in regions where the solution is regular $u_x = \mu x$. The exact gradient is therefore $J_a(a) = \mu a + a\mu$ to be compared with the incomplete gradient μa. We see that the sign of the incomplete gradient is always correct and there is only a factor of 2 missing; something which is not important when using an optimal descent step size in minimization. Obviously, the condition for this analysis to hold for any functional of the form $f(a)g(u)$ where u is the solution of equation (5.3) is that there exists $\varepsilon > 0$ such that $(\log(g))_a = \varepsilon(\log(f))_a$. Something we can verify *a priori* before using the incomplete sensitivity in optimization. Other analytical examples of the comparison of incomplete and exact sensitivities are shown by Mohammadi and Pironneau (2001).

Another interesting example is to consider the sensitivity analysis for an expression of the form $p(x)u_\infty n(x)$ with respect to a parameterization x (for sake of simplicity, we formally consider the case of scalar quantities). This expression appears in the definition of the aerodynamic drag coefficient for instance. Suppose the pressure is given by the Newton formula $p = p_\infty(u_\infty n)^2$. We, therefore, have $pu_\infty n = p_\infty(u_\infty n)^3$. The gradient of this expression with respect to x is:

$$\frac{\mathrm{d}(pu_\infty n)}{\mathrm{d}x} = (pu_\infty)\frac{\mathrm{d}n}{\mathrm{d}x} + \frac{\mathrm{d}p}{\mathrm{d}x}(u_\infty n) = 3p_\infty u_\infty (u_\infty n)^2 \frac{\mathrm{d}n}{\mathrm{d}x}.$$

On the other hand, the incomplete sensitivity is given by:

$$\frac{\mathrm{d}(pu_\infty n)}{\mathrm{d}x} = (pu_\infty)\frac{\mathrm{d}n}{\mathrm{d}x} = p_\infty u_\infty (u_\infty n)^2 \frac{\mathrm{d}n}{\mathrm{d}x}.$$

We see that the two gradients have the same sign and that there is a factor of 3 missing in the incomplete sensitivity. From a fluid dynamic point of view, this is a worst case as we know that small changes in the geometry in high curvature area where the Newton model is valid (leading edges for instance) have important effects on the flow, much more than changes in area where the shape is flat.

The above expression can be rewritten as

$$pu_\infty n = p|u_\infty| \cos\left(\frac{u_\infty}{|u_\infty|} n\right).$$

The incomplete gradient is therefore

$$p(u_\infty n)_x = -p|u_\infty| \sin\left(\frac{u_\infty}{|u_\infty|} n\right) = 0$$

when n is aligned with u_∞. The incomplete sensitivity fails therefore for these area (e.g. area near the leading edge for instance for an airfoil at no incidence). In the same way, if we were interested by the evaluation of the lift sensitivity, the incomplete sensitivity would be wrong where n is close to $u_\infty^\perp$ (e.g. along the intrados and extrados of an airfoil at no incidence). This means that the incomplete sensitivity is not suitable for lift sensitivity evaluation, except if the deformation is along the normal to the shape as in that case the $(\partial p/\partial n = 0)$ boundary condition would imply that the incomplete and exact gradients are the same. This is also why we advocate the use of deformations normal to the wall as parameterization through a CAD-free framework. Below, we reconsider this analysis for the sensitivity of sonic boom with respect to the shape.

5.2 Reduced complexity models and incomplete sensitivities

One way to cheaply improve the incomplete evaluation of sensitivities is to use the linearization of reduced complexity models to approximate the last term in equation (5.2). In other words, consider the following reduced model for the definition of $\tilde{U}(x) \sim U(q(x))$. Suppose for instance $\tilde{U}$ is the Newton formula for the pressure and U the pressure from the Euler system. Consider the following approximate simulation loop:

$$x \to q(x) \to \tilde{U}(x)\left(\frac{U(q(x)}{\tilde{U}(x)}\right). \tag{5.4}$$

The incomplete gradient of J with respect to x can be improved by evaluating the last term in equation (5.2), linearizing equation (5.4) instead of equation (5.1), and by freezing $U/\tilde{U}$.

$$\frac{\mathrm{d}J}{\mathrm{d}x} \sim \frac{\partial J(U)}{\partial x} + \frac{\partial J(U)}{\partial q}\frac{\partial q}{\partial x} + \frac{\partial J(U)}{\partial U}\frac{\partial \tilde{U}}{\partial x}\frac{U(q(x)}{\tilde{U}(x)}. \tag{5.5}$$

$(x \to \tilde{U})$ model is only used in the definition of the gradient and not the state. The reduced model needs to be valid only over the support of the control parameters.

A simple example shows the importance of the scaling introduced in equation (5.4). Consider $U = \log(1+x)$ scalar for simplicity and $J = U^2$ with $\mathrm{d}J/\mathrm{d}x = 2UU' = 2\log(1+x)/(1+x) \sim 2\log(1+x)(1-x+x^2\ldots)$ and consider $\tilde{U} = x$ as the reduced complexity model, valid around $x = 0$. Without the scaling factor incomplete sensitivity gives $J' \sim 2U\tilde{U}' = 2\log(1+x)$ while after introducing the local correction $J' \sim 2U\tilde{U}'(U/\tilde{U}) = 2\log(1+x)(\log(1+x)/x) \sim 2\log(1+x)(1-x/2+x^2/3\ldots)$. Here the scaling is taken linear in U but higher order approximations can be introduced as well.

5.3 Sensitivity of sonic boom to the near field pressure

Consider the simulation loop for the calculation of a cost function to measure the sonic boom for a given parameterization x of the shape:

$$B(x) : x \to q(x) \to p_H \to p_g(p_H, \text{ atmosphere prop.}) \to B(p_g),$$

where p_H is the near field pressure distribution at altitude H which is a function of the state variables (solution of the Euler equations) and p_g solution of the waveform propagation method on the ground.

The gradient of B with respect to x requires the linearization of the different operators involved:

$$\frac{\mathrm{d}B}{\mathrm{d}x} = \frac{\partial B}{\partial p_g}\frac{\partial p_g}{\partial p_H}\frac{\partial p_H}{\partial q}\frac{\partial q}{\partial x}. \tag{5.6}$$

This evaluation is of course expensive when the dimension of the control space is large. Usually an adjoint approach is used to make the cost of the evaluation independent of the size of the control space (Alonso *et al.*, 2002; Mohammadi and Pironneau, 2001). This is performed in particular in the case of steady flows where the storage of intermediate states is not required and the adjoint is developed around the steady-solution. This can be performed in both continuous or discrete forms using automatic differentiation (AD).

In the context of sonic boom evaluation using the waveform propagation method, due to coalescing shocks, one would prefer to perform the adjoint development in the discrete and not continuous level using automatic differentiation in reverse mode. Indeed, the non-differentiability of some operators involved and the presence of discontinuity are naturally taken into account in this approach. This is because in discrete form a discontinuity is always represented by a continuous function. In any event, it would be necessary to save all intermediate solutions of the waveform parameter method between the flight altitude and the ground to be able to integrate backward for the adjoint using the reverse mode of automatic differentiation (Faure, 1996; Gilbert *et al.*, 1991; Griewank, 2001; Mohammadi and Pironneau, 2001; Rostaing *et al.*, 1993).

Sonic boom can be monitored by minimizing, for instance, one of the following functionals:

$$B_{\min} = \left(\frac{I(p_g) - aI(p_g^0)}{I\left(p_g^0\right)}\right)^2, \quad I = \int_{\text{ground}} |\Delta p_g| \mathrm{d}\gamma, \tag{5.7}$$

with $0 < a < 1$ and p_g^0 the pressure signature on the ground for the original shape and

$$B_{\text{inv}} = \alpha \int_{\text{ground}} \left(p_g - p_g^{\text{target}}\right)^2 \mathrm{d}\gamma + \beta \int_{\text{ground}} \left(p_g - p_g^{\text{target}}\right)^\delta \mathrm{d}\gamma, \quad \alpha > 0, \quad \beta > 0,$$

$$\alpha + \beta = 1.$$

where p_g^{target} is a user specified target pressure distribution on the ground. But the target pressure might be unrealizable and the optimization problem without solution.

$B_{\min}$ is a measure of the pressure jumps accumulation on the ground and the aim is to reduce these jumps. a cannot be 0 as we cannot completely remove the boom.

On the other hand, by minimizing B_{inv}, we realize a target pressure signature on the ground having less boom. In B_{inv}, the second integral in the cost function is used to avoid the functional being flat close to the minimum. $0 < \delta < 1$ is also an optimization parameter and has to be chosen. In this work, we consider $\delta = 0.3$. We studied the

importance of such functionals in the work of Cabot and Mohammadi (2002) and Mohammadi and Saiac (2002) for a model problem.

The difficulty with B_{inv} is that the prescribed ground pressure might not be associated to a feasible flow field while $B_{\min}$ does not involve an *a priori* ground pressure distribution. In addition, we will see that $\partial B_{\min}/\partial p_H$ is less sensitive to discrepancies in the near-field flow prediction, due for instance to the mesh quality.

We show the sensitivity of these functionals with respect to the close field pressure distribution in Figure 2.

Once $\partial B/\partial p_H$ is computed (for either $B_{\min}$ or B_{inv}, Figure 3), we evaluate its product with the operator $\partial p_H/\partial x$. This latter evaluation requires the linearization of the Euler system which we would like to avoid. We have two alternatives:

- to use reduced complexity models for sensitivity analysis; and
- to redefine the functional and adapt the problem to the context of incomplete sensitivities.

5.3.1 Reduced complexity models. The first approach to reduce the complexity of the sensitivity analysis is to replace, only for sensitivity analysis, the Euler system by the waveform propagation method, propagating the wall pressure distribution (p_x) directly to the ground (instead of just from altitude H). We insist on the fact that p_x is solution of the Euler system:

$$x \longrightarrow q(x) \longrightarrow p_x \longrightarrow p_g.$$

To compute $\mathrm{d}p_g/\mathrm{d}x$ we need finally to find an approximation linking p_x and the shape x to be used in the linearization (instead of the Euler system). For inviscid flows, in regions of high curvature, a good approximation is given by the Newton formula for

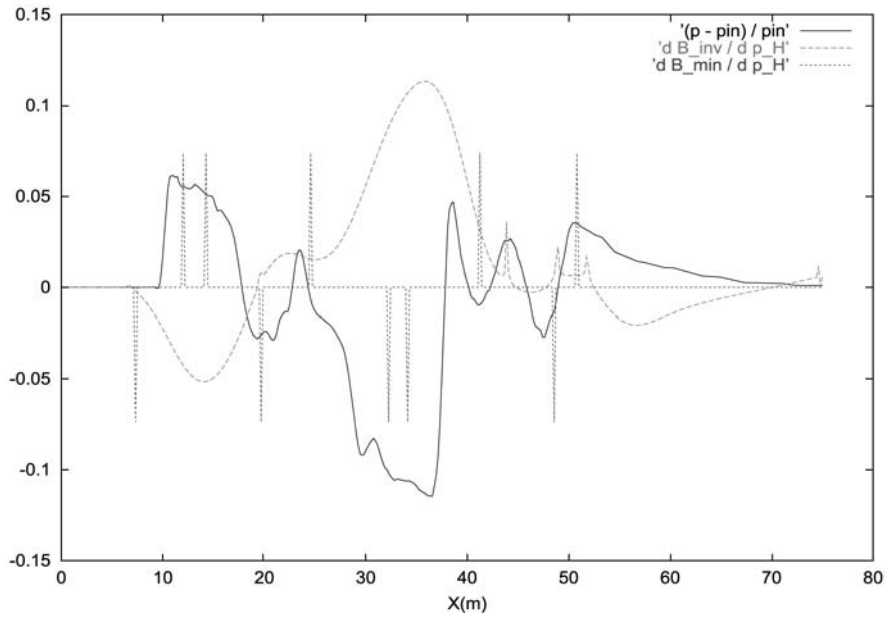

Figure 2.
$\partial B_{\text{inv}}/\partial p_H$ and $\partial B_{\min}/\partial p_H$ superposed on the near-field pressure distribution. $\partial B_{\text{inv}}/\partial p_H$ is rather smooth while $\partial B_{\min}/\partial p_H$ vanishes almost everywhere and only contains Diracs

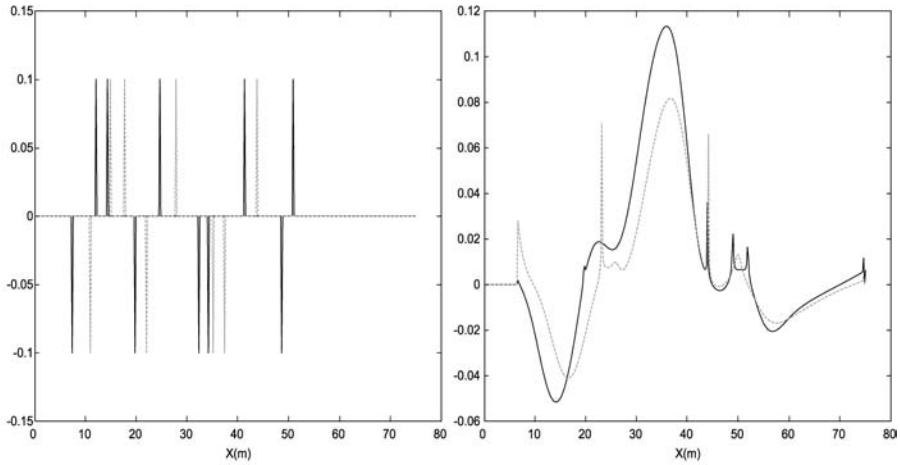

Note: We see that $\partial B_{\min}/\partial p_{\mathrm{H}}$ is less sensitive to the altitude (only a shift is observed in Diracs locations). This also shows that the waveform propagation model is a suitable reduced complexity model, to be considered instead of the Euler system, in the analysis of the sensitivity of sonic boom with respect to the shape

Figure 3.
$\partial B_{\min}/\partial p_H$ (left) and $\partial B_{\mathrm{inv}}/\partial p_H$ (right) based on two cross-sections close (plane curves) and far (dashed curves) from the aircraft

the pressure distribution over walls. We account therefore only for the effect of the pressure distribution on the shape on the near field pressure signature. We have to account therefore for the part of the boom coming from the shocks away from the wall. We will see that, by keeping the shocks bow (by opposition to attached) and the leading edges as smooth or rounded (by opposition to sharp) as possible, this requirement is satisfied.

6. Cost function definition

The functionals $B_{\min}$ and B_{inv} accounting for the sonic boom have been introduced above. In this work, we also consider constraints on aerodynamic coefficients as well as geometric characteristics of the aircraft.

More precisely, we consider the problem of drag (C_{d}) minimization with constraints on the lift (C_{l}), volume (V) and maximum by-section thickness (d) defined for each node. In our approach, the mesh is unstructured and the surface mesh is made of triangles. In the by-section definition of the shape the number of sections is arbitrary and depends on the complexity of the geometry. The sections are obtained by intersecting vertical planes with the shape. The maximum thickness d of each section is evaluated. Then, each node in the surface mesh is associated with two sections and linear interpolation is used to define the maximum by-section thickness associated this node (Figure 4). The cost function is given by:

$$J(x) = |C_{\mathrm{d}} - C_{\mathrm{d}}^{\mathrm{des}}| + \left(C_{\mathrm{l}}^{0} - C_{\mathrm{l}}\right)_{+} + (V^{0} - V)_{+} + \int_{\mathrm{shape}} |\mathrm{d} - \mathrm{d}^{0}| \mathrm{d}\gamma + B(x).$$

Notation 0 denotes initial shape values. $C_{\mathrm{d}}^{\mathrm{des}} \leq C_{\mathrm{d}}^{0}$ is the target value for the drag coefficient. $B(x)$ is either $B_{\min}$ or B_{inv} from (5.7). $(\cdot)_{+} = \max_r(0, .)$ where $\max_r$ is a regularized max. The aim is to avoid the volume and lift coefficient from decreasing.

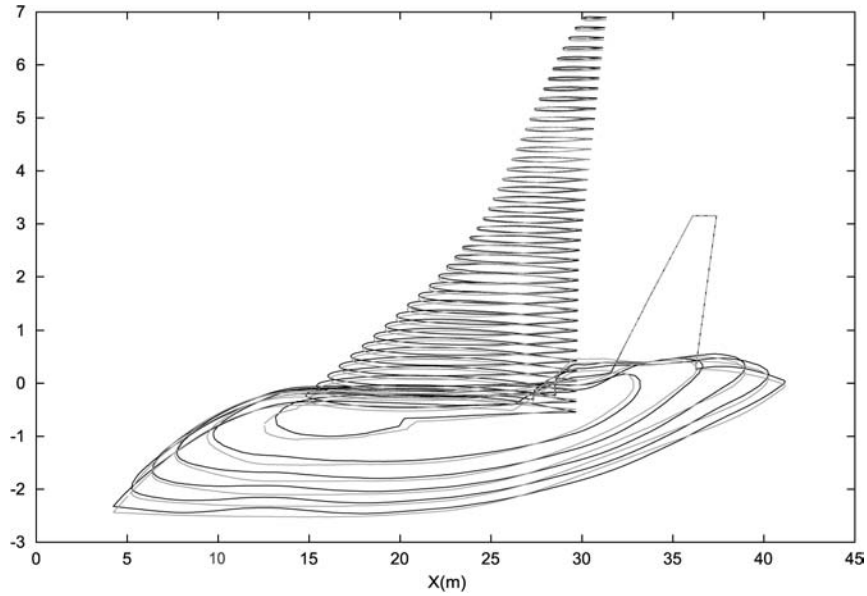

Figure 4.
By-section definition of the shape used to enforce the maximum by-section thickness constraint for the original and optimized aircraft

In addition to the given lift constraint expressed in the cost function by penalty, we use the inflow incidence to enforce the given lift constraint. We know that in cruise condition (far from stall), the lift is linear with respect to the angle of incidence. During optimization the incidence follows the following equation: $\theta^{n+1} = \theta^n - 0.5(C_1^n - C_1^0)$, $\theta^0 = 0$, where n is the optimization iteration.

6.1 Redefinition of J for incomplete sensitivity evaluation

We said that a cost function based on information away from the wall is not suitable for incomplete sensitivity evaluation. In particular, since B_{inv} and $B_{\min}$ are defined on the ground and not on the shape, we propose a reformulation of the functional linking the pressure signature on the ground to wall-based quantities. This is done together with the use of the waveform propagation method for the evaluation of $\partial p_g/\partial x$ as seen above.

We think that bow shocks introduce less pressure jump than attached shocks. Bow shocks are usually associated with smooth geometries. On the other hand, shape optimization based on drag reduction in supersonic regime leads to sharp leading edges. Therefore, to avoid an increase in the boom, it is important to keep the leading edges of the aircraft smooth while doing drag reduction. We introduce the following requirements.

- Specify that the wall near leading edges has to remain smooth. This is monitored through the smoother in the CAD-free framework seen above.
- Ask for the local drag force C_d^{loc} due to the leading edge regions to remain unchanged or to increase while the global drag force decreases.

The cost function becomes therefore:

$$\tilde{J}(x) = |C_d - C_d^{des}| + \left(C_l^0 - C_l\right)_+ + (V^0 - V)_+ + \int_{shape} |d - d^0| d\gamma$$

$$+ \left(\left(C_d^{loc}\right)^0 - \left(C_d^{loc}\right)\right)_+ ;$$

where C_d^{loc} is the measure of the drag force over regions where $\vec{n} \cdot \vec{u}_\infty < 0$ ($\vec{n}$ being the local outward normal to the shape). Introducing a differentiable localization function $f(s^+)$ such that $(0 \leq f(s^+) \leq 1)$, C_d^{loc} is defined as:

$$C_d^{loc} = \frac{2}{\rho_\infty |\vec{u}_\infty|^2} \int_{shape} p \cdot \vec{n} \cdot \vec{u}_\infty f(s^+) \, d\Gamma, \quad s^+ = \frac{\vec{n} \cdot \vec{u}_\infty}{|\vec{n} \cdot \vec{u}_\infty|}.$$

This differentiable localization term is used to avoid non-differentiability for C_d^{loc} and to allow for integration over the whole shape.

In addition to the previous modification of the functional, we introduce regularity requirements for areas where $(f(s^+) \neq 0)$. This is monitored through the smoothing operator available in the CAD-free parameterization.

7. Full aircraft optimization

We consider a supersonic business jet geometry provided by Dassault Aviation company (Figures 5 and 6). The cruise speed is Mach 1.8 at zero incidence and the flight altitude is 55,000 ft. The results show the performance of the optimization method including the validity of the incomplete sensitivity approach and the reformulation of the functional we use for this configuration.

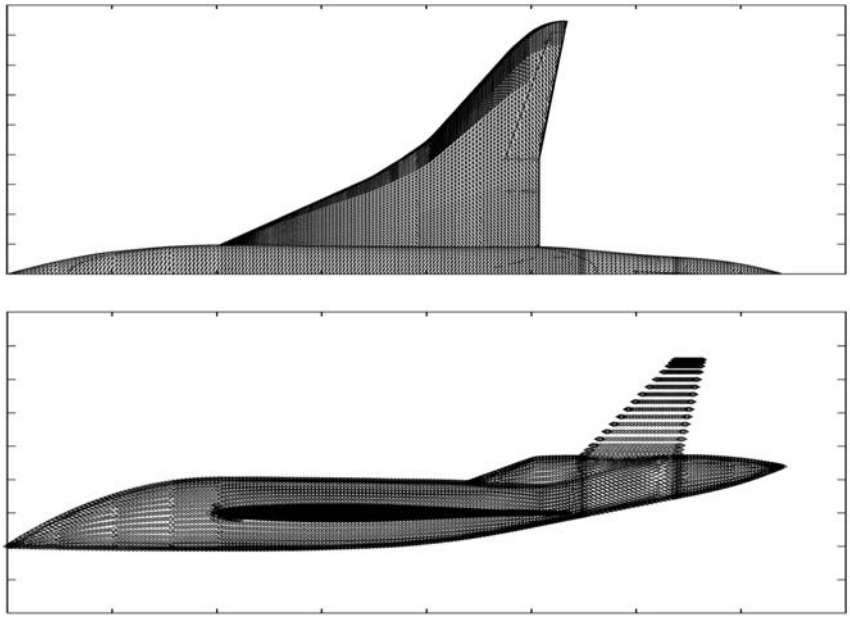

Figure 5.
Upper and side views of the SSBJ discretization, all these nodes are control parameters

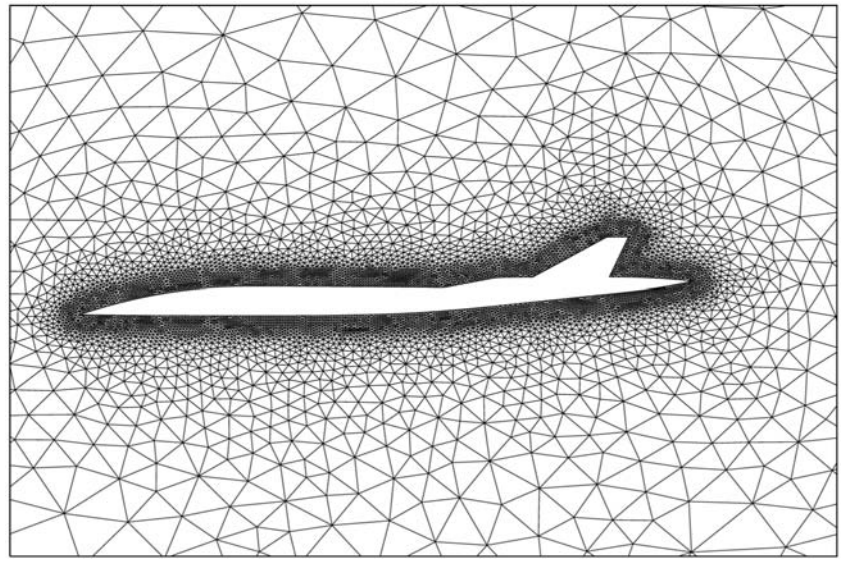

Figure 6.
Partial view of the CFD mesh in the symmetry plane

We performed 1,000 steepest descent minimization iterations. At each iteration, an incomplete evaluation of the state (ten explicit Runge-Kutta iterations of the Euler solver) is performed. The global cost of this optimization is comparable to one flow analysis with this code (about 10,000 explicit RK iterations) and takes about 4 h on a 1 GHz PC with 500 Mb RAM. The extra cost in optimization compared to pure simulation due to incomplete sensitivity analysis, shape and mesh deformation, minimization algorithm, etc. is negligible. In Figure 7, we show a cross-section of the

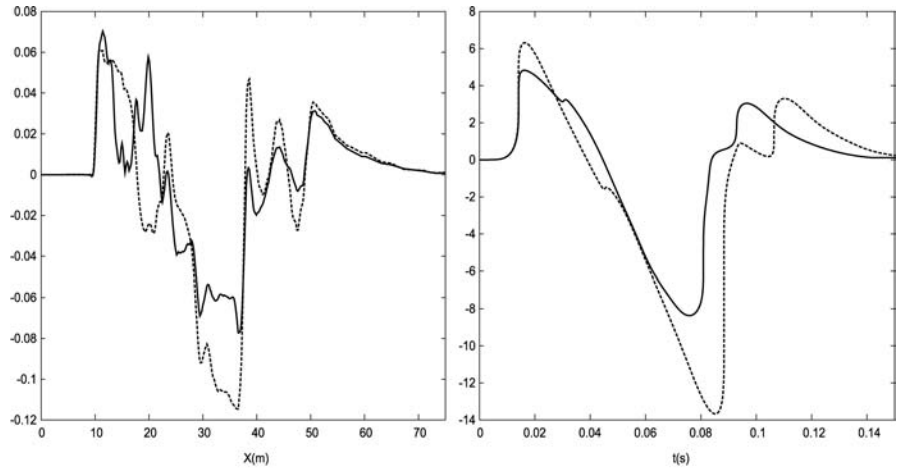

Note: We observe a non trivial impact of the modification of the near-field pressure distribution on the ground pressure

Figure 7.
Cross-section of the near-field CFD pressure variations ($p - p_\infty/p_\infty$) in the symmetry plane (left) and the corresponding ground pressure signatures (right) for the initial (dashed curves) and optimized (continuous curves) shapes

close field CFD pressure signature close to the aircraft in the symmetry plane and the ground pressure signature for the initial and optimized shapes. Figure 8 shows upper and lateral views of aircraft surface iso-Mach contours. Figure 9 shows iso-contours of normal deformations with respect to the original shape. During optimization, the drag has been reduced by 20 percent while the lift has been increased by 10 percent. Geometric constraint on the volume and maximum cross-section thickness has been satisfied and the value of $C_{\mathrm{d}}^{\mathrm{loc}}$ maintained (Figure 10).

8. Concluding remarks

Shape optimization in a CAD-free framework using incomplete state and gradient evaluations has been presented for a multi-criteria optimization problem involving requirements on the acoustic, aerodynamic and geometric characteristics of jetliners. It has been shown that this platform is suitable for such a realistic design and that the complexities of the optimization and simulation are now comparable. In particular, it has been shown that incomplete sensitivities give satisfactory results after a reformulation of the cost functional. This enables a better understanding of sonic boom

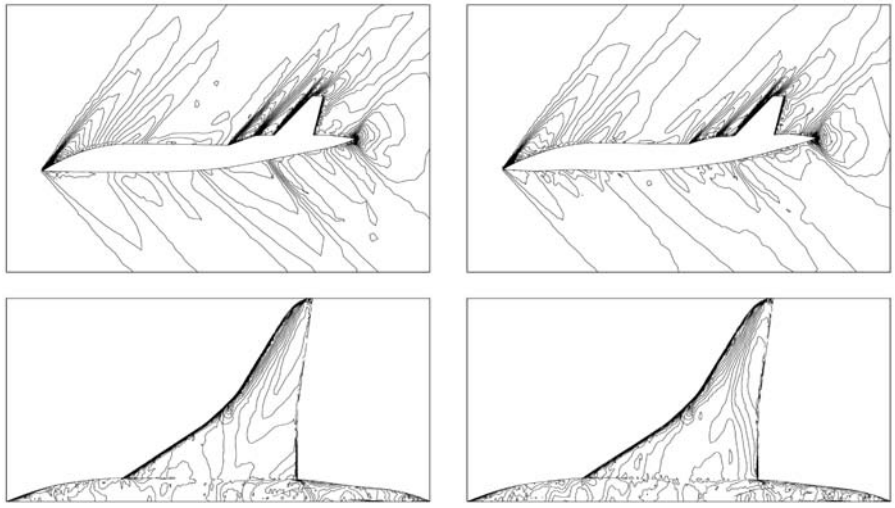

Figure 8.
Upper: near-field iso-Mach contours for the initial and optimized aircraft in the symmetry plane. Lower: Upper surface iso-Mach contours for the initial and optimized aircraft

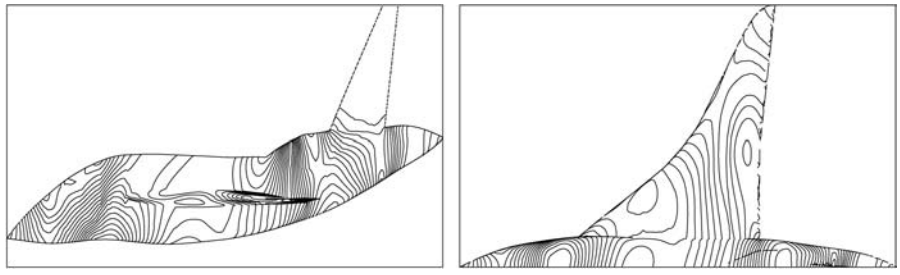

Figure 9.
Iso-contours of normal deformation with respect to the original shape

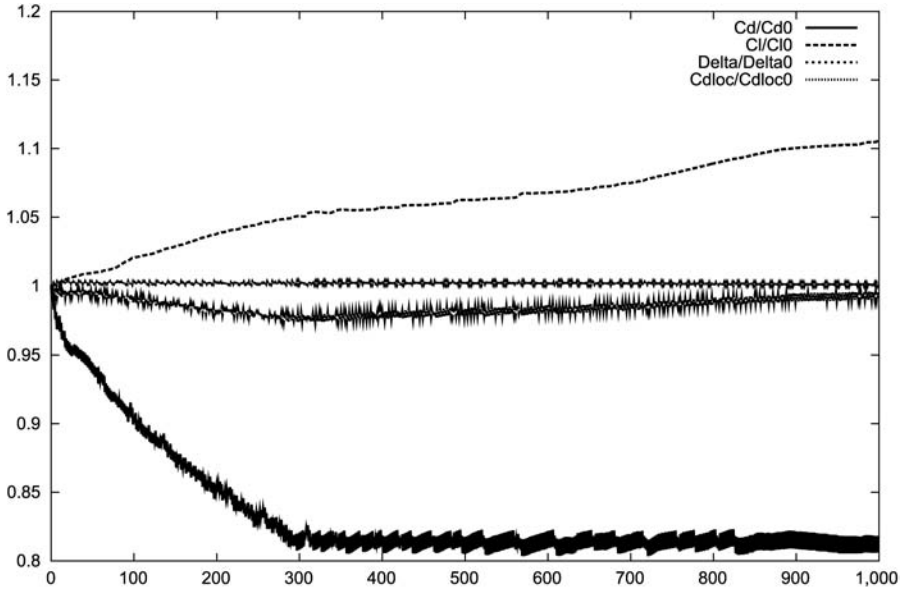

Note: The drag has been reduced by 20 percent while the lift has been increased, geometric constraints satisfied and C_d^{loc} maintained

Figure 10.
Evolution of C_d/C_d^0, C_l/C_l^0, $(\int(d-d^0)/(\int d^0)$ and $C_d^{loc}/(C_d^{loc})^0$

origins and mechanisms, and provides useful input to the design of future supersonic civil transports with a controlled boom and reduced drag. In addition, this approach is suitable in the context of black-box commercial simulation softwares as no linearization is required for the state equation.

References

Alonso, J.J., Kroo, I.M. and Jameson, A. (2002), "Advanced algorithms for design and optimization of QSP", AIAA Paper 2002-0144.

Faure, C. (1996), "Splitting of algebraic expressions for automatic differentiation", *Proc. of the Second SIAM Workshop on Computational Differentiation*, July, Santa Fe, NM.

Farhat, C., Degand, C., Koobus, B. and Lesoinne, M. (1998), "Torsional springs for two-dimensional dynamic unstructured fluid meshes", *Computer Methods in Applied Mechanics and Engineering*, Vol. 163, pp. 231-45.

Gilbert, J.C., Le Vey, G. and Masse, J. (1991), "La différentiation automatique de fonctions représentées par des programmes", INRIA research report 1557, Rocquencourt, France.

Griewank, A. (2001), *Computational Differentiation*, Springer, New York, NY.

Mohammadi, B. (1994), *CFD with NSC2KE: User-guide*, Technical note INRIA 164, Rocquencourt, France.

Mohammadi, B. and Cabot, A. (2002), "Incomplete sensitivities and cost function reformulation leading to multi-criteria investigation of inverse problems", *Optimal Control: Applications and Methods*, Vol. 24 No. 2, pp. 73-84.

Mohammadi, B. and Pironneau, O. (2001), *Applied Shape Optimization for Fluids*, Oxford University Press, Oxford.

Mohammadi, B. and Saiac, J.H. (2002), *Pratique de la simulation numérique*, Dunod, Paris.

Polak, E. (1997), *Optimization: Algorithms and Consistent Approximations*, Springer, New York, NY.

Rostaing, N., Dalmas, S. and Galligo, A. (1993), "Automatic differentiation in Odyssee", *Tellus*, Vol. 45a No. 5, pp. 558-68.

Thomas, Ch. L. (1972), *Extrapolation of sonic boom pressure signatures by the waveform parameter method*, Nasa TN. D-6832.

Whitham, G.B. (1952), "The flow pattern of a supersonic projectile", *Comm. Pure Appl. Math.*, Vol. 5 No. 3, pp. 301-48.